Influence of ZnF2 and ZnCl2 on luminescence investigations and crystal field calculation of Eu3+ doped zinc oxide-phosphate glasses

Samah Amrouch, Rekia Belhoucif, Mohand Chalal, Matias Velázquez, Yannick Guyot, Omar Lamrous

Version of Record: https://www.sciencedirect.com/science/article/pii/S0925346722004219
Manuscript_05452d49e43b117a98a909289dacc407

Influence of ZnF_2 and $ZnCl_2$ on Luminescence investigations and crystal field calculation of Eu^{3+} doped zinc oxide-phosphate glasses

Samah Amrouch [*,A,B], Rekia Belhoucif [C, D,E], Mohand Chalal [C,F], Matias Velázquez[B], Yannick Guyot [G], Omar Lamrous [A]

[A] Laboratoire de Physique et Chimie Quantique (LPCQ), Université Mouloud Mammeri Tizi-Ouzou, BP 17 RP, 15000 Tizi-Ouzou, Algeria
[B] Univ. Grenoble Alpes, CNRS, Grenoble INP, SIMAP, 38000, Grenoble, France
[C]Faculté de Physique, Laboratoire d'Électronique Quantique, USTHB, BP 32 El alia, 16111 Bab Ezzouar, Alger, Algeria
[D]Faculté des Sciences, Département de Physique, UMBB, Route de la Gare Ferroviaire, 35000, Boumerdes, Algeria
[E]Laboratoire Revêtement, Matériaux et Environnement, UMBB, Boumerdes, Algeria
[F]Laboratoire CSPBAT, CNRS (UMR 7244), Université Sorbonne Paris Nord, UFR SMBH, 74 rue Marcel Cachin, 93017 Bobigny, France
[G] Institut Lumière matière (ILM),UMR-CNRS 5306, Université Lyon1, F-69622 Villeurbanne Cedex, France

E-mail: *amrouch.samah@ummto.dz

Abstract: A series of Eu^{3+}-doped $70NaPO_3$-$20ZnO$-$10(ZnF_2$ / $ZnCl_2)$ glasses were prepared by conventional melting quenching method.The samples were characterized by differential scanning calorimetry (DSC), X-ray diffraction (XRD), electron probe microanalysis (EDS/WDS) and optical spectroscopy. Using the emission spectra a set of Judd-Ofelt (JO) intensity parameters (Ω_2, Ω_4, Ω_6) was refined, which in turn permitted to calculate transition probabilities (A_{ED}, A_{MD}), branching ratios (β), radiative lifetimes (τ_{rad}) and stimulated emission cross-sections for the $^5D_0$-^7F_J transitions. The relative luminescence intensity ratio of $^5D_0$-$^7F_2$-$^5D_0$-$^7F_1$ transitions has been evaluated to estimate the local site symmetry around the Eu^{3+} ions. Second and fourth rank crystal-field (CF) parameters together with the CF strength parameter have been reported for the first time for such study by assuming the C_{2v} symmetry for the Eu^{3+} ions in both the phosphate glasses. Large stimulated emission cross-section, high branching ratios and quantum efficiencies (~80%), also, intense red luminescence at 616 nm confirm that these present glasses suggesting for visible red lasers materials and optical devices.

Keywords: Eu^{3+} ion spectroscopy, phosphate Glasses, Judd-Ofelt theory, Second and fourth rank crystal-field.

1. Introduction

Rare-earth doped materials have a wide range of practical uses, which encourages the development of novel materials. Eu^{3+}-doped crystals or glasses are promising materials for photonic devices and optoelectronics as optical amplifiers, optical communications, laser materials, sensors, high density and optical memory devices **[1-7].** The choice for Eu^{3+} cations to dope materials is due to their narrow emission band, longer excited-state lifetimes, almost monochromatic light with excellent red emission efficiency, due to its hypersensitive $^5D_0$-$^7F_2$ radiative emission transition at 612 nm, and purely MD emission transition at 593 nm corresponding to the $^5D_0$-$^7F_1$ transition **[8-9].**

The chemical composition of the glass host plays a very important role in the determination of the spectroscopic characteristics of Eu^{3+} ions. Among various glasses, phosphate glasses have attracted much attention due to their low melting points, high transparency, and their ability to dissolve rather high concentrations of rare earth ions before the quenching effect comes into play **[10-12]**. However, these hosts are chemically unstable, and their hygroscopic behavior constitutes a disadvantage for their long-term use under normal atmospheric conditions **[10-14].** Addition of alkaline oxide such as (ZnO, BaO, SrO..) in phosphate glasses increases the thermal stability and the transparency in the UV- Visible spectral ranges, also helps to distribute Ln^{3+} ions throughout the matrix, preventing non-radiative relaxations which increasing fluorescence emission **[15-16].** Additives such as fluorides (ZnF_2,BaF_2,PbF_2…) and chlorides ($ZnCl_2$,$PbCl_2$…) in phosphate

host are used to tailor their chemical composition, which also increases the radiative emission of the fluorescent level**[9-12].**

Combinations of the zinc oxide-chlorid $ZnO\text{-}ZnCl_2$ and zinc oxide-fluoride $ZnO\text{-}ZnF_2$ constituents, result exellent changes of optical and spectral performance of phosphate glasses .In this work, our contribution focuses on the effect of the additives $ZnCl_2$ and ZnF_2, in Eu^{3+} doped $NaPO_3$-ZnO glasses composition, on the optical and spectroscopic properties. A series of experimental measurements were performed, which include absorption spectra in the UV-Visible and IR spectral ranges, chemical analysis by electron probe microanalysis with wavelength dispersion spectroscopy (EPMA/WDS), energy dispersive spectroscopy (EDS), X-ray diffraction (XRD), differential scanning calorimetry (DSC) and emission spectroscopy. Finally, from the emission spectra, the Judd-Ofelt intensity parameters $\Omega_{k=2,4,6}$ and the "laser" spectroscopic parameters (β, τ_{rad}, A_{ED}, A_{MD}) were estimated. The luminescence decay of the $^5D_0 \rightarrow {}^7F_2$ transition was also analyzed.

2. Experimental

Phosphates glasses samples with chemical composition: $70NaPO_3+20ZnO+10ZnF_2+0.5Eu_2O_3$ and $70NaPO_3\text{-}20ZnO\text{-}10ZnCl_2+0.5Eu_2O_3$ (in mol%) (hereafter, named as $PNZFEu_{0.5}$ and $PNZClEu_{0.5}$ respectively **[17]**), have been obtained by melt quenching method . High purity powders were used: $NaPO_3$ (>99%), ZnO (>99.9%), ZnF_2(>98%), $ZnCl_2$(>98%), Eu_2O_3 (99.9%). Each chemical composition batch amounts were calculated to yield 4g-glasses. The homogeneously mixed powders were melted in a covered platinum crucible at 950-1100°C, depending on the composition, by means of an electric furnace at ambient atmosphere for about 30 min to 1h.The obtained glass samples were immediately introduced into an annealing furnace, preheated just below the glass transition temperature T_g-20 *°C*, and annealed for 2 h, in order to reduce the thermal and mechanical strains. The glasses thus obtained were polished to measure their structural, optical and spectroscopic properties.

The room temperature absorption spectra were obtained for all samples in the 200-2500 nm spectral range, with a Perkin Elmer UV-VIS-NIR spectrophotometer. The density of the prepared glasses was measured using Archimedes principle, with distilled water as immersion liquid. The Eu^{3+} contents were determined by EPMA/WDS and EDS. In the remainder of this paper, we shall use an average concentration of 1.763×10^{20} $Eu^{3+}.cm^{-3}$ for $PNZFEu_{0.5}$ and 1.689×10^{20} $Eu^{3+}.cm^{-3}$ for $PNZClEu_{0.5}$.

The differential scanning calorimetry analyses of the glasses were performed by means of a differential thermal analyser DSC Mettler Toledo, with a heating rate of 10 *°C /min*. The samples were heated using stainless steel crucibles in a temperature range of 25 *°C* to 750 *°C* under N_2 atmosphere with a (60 ml/min) flow. The X-ray diffraction was carried out in a powder diffractometer (MPD PANalytical X'pert Pro), in the 2θ range 8-100° with Cu K_α radiation (λ=1.54056 *Å*), operating at (40 kV and 30 mA). Emission spectra at room temperature (RT) and low temperature (LT, 77 *K*) were recorded in the visible under pulsed excitation at 465, 525 and 575 nm from an OPO laser (EKSPLA NT342, 10 *Hz*, 7 *ns*) associated with an ANDOR ICCD camera. The emission spectra are not corrected for spectral and amplitude sensitivity. Luminescence decay curves were recorded at RT and LT with the help of either a R928 AsGa (Research Inc.) photomultiplier tubes coupled with a Wave Runner 64Xi Lecroy digital oscilloscope, in the visible spectral ranges, corresponding to the $^5D_0 \rightarrow {}^7F_2$ emission transition at 612 nm and by exciting the sample at 465 nm using the same pulsed tuneable OPO laser. Using the Fresnel's expression relating optical transmission coefficient and linear refractive index ($T=2n/(n^2+1)$), an estimate of the linear refractive index was performed**.** The average linear refractive index obtained is 1.60 for the two glasses.

3. Results and discussions

3.1. Thermal stability of $PNZFEu_{0.5}$ and $PNZClEu_{0.5}$ glasses

Figure 1 displays the DSC curve of $PNZFEu_{0.5}$ and $PNZClEu_{0.5}$ glass hosts. The measured characteristic temperatures were the transition temperature T_g, the starting point of crystallization temperature T_X, the crystallization temperature T_c of glass hosts, and they are listed in **Table 1**.In order to evaluate thermal stability against *devitrification*, a temperature difference is usually employed as follows: **$\Delta T=Tx-T_g$[18-19].** We found that these glasses are thermally stable (*$\Delta T > 120°C$*, see **Table 1**).By comparison between the two samples, it can be seen that the addition of ZnF_2 in the phosphate structure allows to have Tg and T_x much higher than those obtained with the addition of $ZnCl_2$. This result allows us to conclude that the addition of ZnF_2 increases the thermal stability of phosphate glasses.

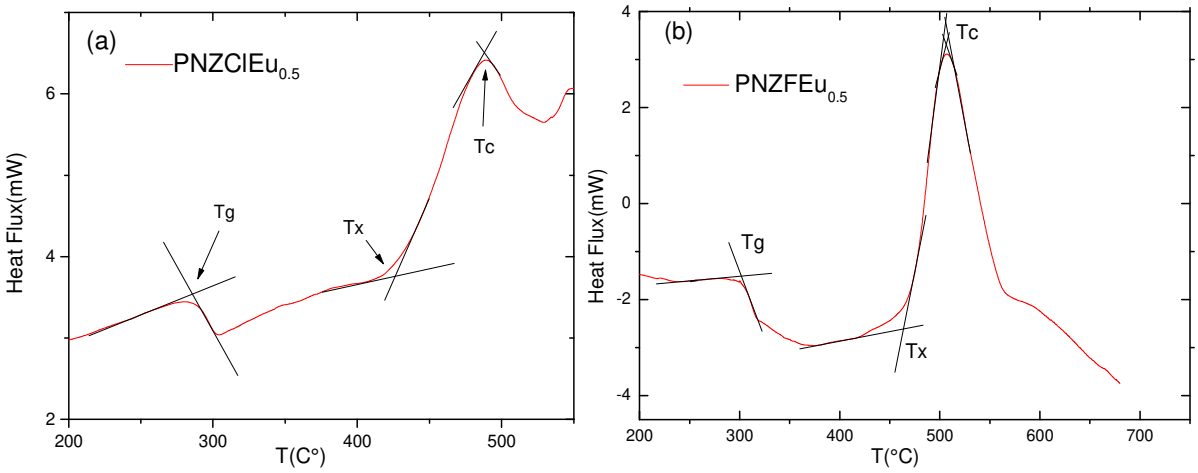

Figure 1 DSC curves of (a) $PNZClEu_{0.5}$ and, (b) $PNZFEu_{0.5}$ glass samples.

Table 1 Thermal properties of $PNZFEu_{0.5}$ and $PNZClEu_{0.5}$ glass samples. T_g, T_x and T_c represent the glass transition temperature, the starting point of crystallization temperature, the crystallization temperature, respectively, and $\Delta T=T_x-T_g$.

Glass	**T_g (°C)**	**T_x(°C)**	**T_c(°C)**	**ΔT(°C)**
$PNZClEu_{0.5}$	286	427	488	141
$PNZFEu_{0.5}$	302	464	506	162

3.2. X-ray diffraction (XRD) glasses

Fig. 2 shows the X-ray diffraction patterns (XRDs), of the $PNZFEu_{0.5}$ and $PNZClEu_{0.5}$ glass samples prepared. The absence of any sharp peak, and a broad diffusion at low angles, is typical of long-range structural disorder, can assess the amorphous nature of the glasses **[20-21]**. While the thermal annealing at 380 °C for 1 hour shows some diffraction peaks indicating its tendency towards crystallinity (**Fig.2**). The research of the glass ceramic is in progress by a thermal treatment refinement.

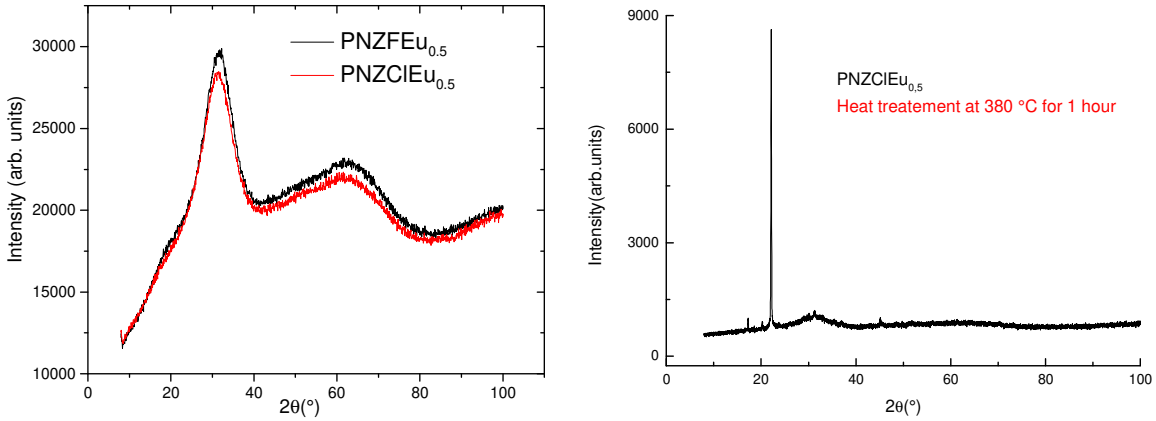

Figure 2 X-ray diffraction patterns of $PNZFEu_{0.5}$ and $PNZClEu_{0.5}$ glasses (at left) and $PNZClEu_{0.5}$ glass annealing at 380 °C for 1h (at right).

3.3. Band gap and Urbach energy

The absorption due to the band-to-band transition of amorphous materials can be analyzed using optical band gap **[22]**. From absorption spectra, we can estimate the optical band gap (E_{opt}) for the glasses, using Davis and Mott rule **[23]**:

$$\alpha(\nu) = \frac{A(h\nu - E_{opt})^n}{h\nu} \qquad (1)$$

where A is a proportionality constant, E_{opt} is the optical energy gap, hυ is the incident photon energy and n is an index which depends on the nature of the transition : indirect when n=2, or direct for n=1/2. The plots of $(\alpha h\upsilon)^{1/2}$ and $(\alpha h\upsilon)^2$ as a function of photon energy (hυ) of the glasses are shown in Fig. 3. The E_{opt} of $PNZFEu_{0.5}$ and $PNZFEu_{0.5}$ glasses, can be calculated from the linear portion of the curves by extrapolating them to cross the hυ axis at $(\alpha h\upsilon)^{1/2} = 0$ and $(\alpha h\upsilon)^2 = 0$, respectively. The optical band gaps are shown in Table 2. For a fixed molar proportion of ZnO (20 %), the substitution of $ZnCl_2$ or ZnF_2 for $NaPO_3$ leads to the direct gap variation from 4.48 to 4.52 eV and from 4.30 to 4.37 eV for indirect gap, respectively. These glass systems have a higher optical band gap values than TBLFE **[22]** and EuSr10ZnPbP **[21]** reported glasses. The higher value of the optical band gap confirms the insulating nature of the $PNZFEu_{0.5}$ and $PNZClEu_{0.5}$ glass systems **[21]**. In many crystalline and amorphous materials, the α(υ) depends exponentially on hυ, and this exponential dependence is expressed by Urbach's equation **[22]** :

$$\alpha(\nu) = \alpha_0 \exp\left(\frac{h\nu}{E_U}\right) \qquad (2)$$

where α_0 is a constant and E_U is the Urbach energy. The E_U can be obtained from the curve ln (α) versus hυ shown in the inset of Fig. 3. The Urbach energy values are found to be 0.34 eV for $PNZFEu_{0.5}$ and 0.35 eV for $PNZClEu_{0.5}$, respectively. These values are similar to EuSr10ZnPbP **[21]** system, and higher than TBLFE **[22]** glass. The increase of E_U indicates a higher number of defects in the glass systems **[21]**.

Table 2 The direct (n=1/2), and indirect (n=2) band gap and Urbach energy of $PNZFEu_{0.5}$ and $PNZClEu_{0.5}$ glasses.

Samples	Direct Band gap (eV)	Indirect band gap (eV)	Urbach energy (eV)	Ref
$PNZFEu_{0.5}$	4.52	4.37	0.34	[Present work]
$PNZClEu_{0.5}$	4.48	4.30	0.35	[Present work]
EuSr10ZnPbP	4.45	4.04	0.37	**[21]**
TBLFE	2.69	2.62	0.24	**[22]**

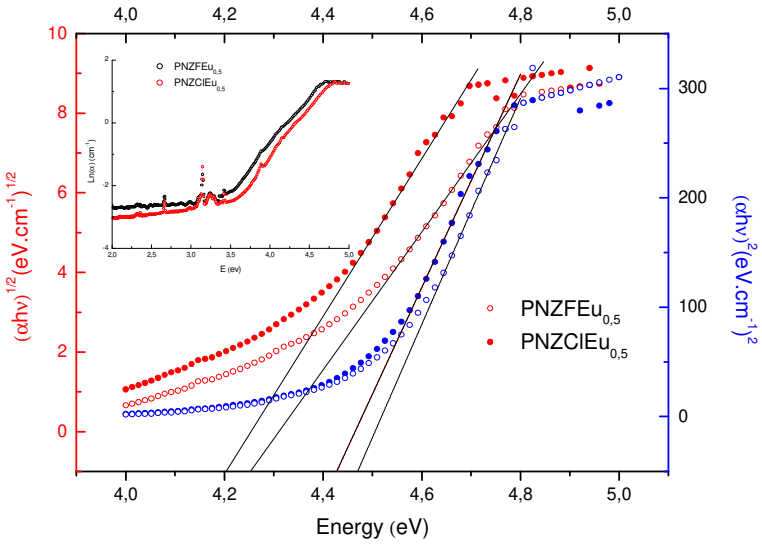

Figure 3 Variation of the optical band gap for direct and indirect transition in the $PNZFEu_{0.5}$ and $PNZClEu_{0.5}$ glasses. The inset is the Urbach energy of $PNZFEu_{0.5}$ and $PNZClEu_{0.5}$ Glasses.

4. Absorption spectra

The absorption spectra of $0.5Eu_2O_3$ doped PNZF, PNZCl glasses for UV-VIS and NIR regions are shown in Fig 4.The absorption spectrum presents five absorption bands that are attributed to the absorption transitions from the ground state $^7F_0$ to the excited states $^5G_2$ $^5D_2$, $^5D_1$, $^5L_6$, and $^7F_6$, respectively. The $^7F_0 \rightarrow {}^5D_J$ absorption bands are weak due to spin-forbidden rule. In contrast, the $^7F_{0,\ 1} \rightarrow {}^7F_6$ levels lying in the IR region are stronger and are well resolved owing to spin-allowed rule. The absorption band assigned as $^7F_0$-$^5L_6$ is found to be more intense than the other transitions, though it is forbidden by the ΔS and ΔL selection rules but allowed by the ΔJ selection rule. The intensity of $^7F_0$-$^5D_1$ magnetic dipole allowed transition is relatively weaker than that of $^7F_0$-$^5D_2$ (hypersensitive transition) induced electric dipole allowed transition for all compositions.

The absorption bands correspond to the f-f optical excitation from ground $^7F_0$ and thermally populated $^7F_1$ levels at the excited states of the Eu^{3+} ion, and they practically overlap. Indeed, the first excited $^7F_1$ free-ion level of Eu^{+3} is only about 380 cm^{-1} above the ground state $^7F_0$. At room temperature, the fractional thermal population of the $^7F_1$ level cannot be neglected: about 66 % of the ions populate the $^7F_0$ level, 32 % the $^7F_1$ level and also about 2 % the $^7F_2$ level. The absorption cross-section at 393.5 nm was determined to be 7.6×10^{-21} cm^2 for both $PNZFEu_{0.5}$ and $PNZClEu_{0.5}$ glasses.

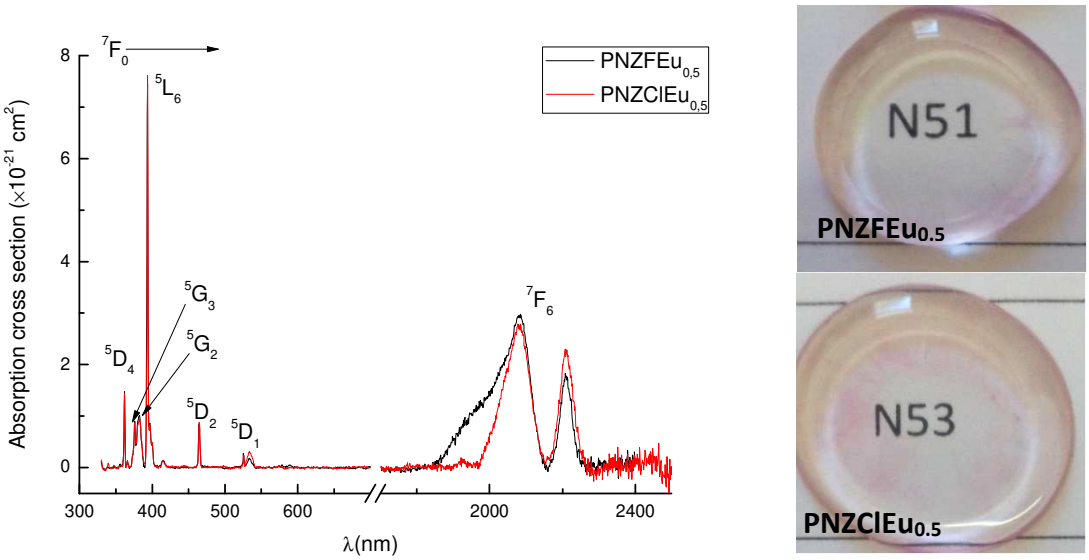

Figure 4 Absorption cross section spectra of Eu^{3+} doped phosphate glasses at room temperature.

5. Emission spectra and Judd Ofelt analysis

Emission spectrum at room and low temperature of $PNZFEu_{0.5}$ and $PNZClEu_{0.5}$ glass measured under a 465 nm laser excitation is shown in Fig. 5. Only emission from the $^5D_0$ level was occurring, owing to the efficient multiphonon relaxation from the higher ^5D_J levels to the $^5D_0$ level. The spectra consists of the well-known $^5D_0$-^7F_J (J= 0, 1, 2, 3, 4, 5 and 6) transitions namely $^5D_0$-$^7F_0$ (579 nm), $^5D_0$-$^7F_1$ (592 nm), $^5D_0$-$^7F_2$ (616 nm), $^5D_0$-$^7F_3$ (655 nm) and $^5D_0$-$^7F_4$ (699 nm), $^5D_0$-$^7F_5$ (750 nm), $^5D_0$-$^7F_6$ (814 nm). Generally, the orange emission due to $^5D_0 \rightarrow {}^7F_1$ transition dominates when Eu^{3+} ions prefer to occupy the inversion symmetry sites, whereas the red emission originating from $^5D_0 \rightarrow {}^7F_2$ transition is predominant when these ions reside in a highly asymmetric environment **[24]**. Thus, intensity of these transitions is a measure of the local environment of Eu^{3+} ions. In addition, the hypersensitive transition $^5D_0$-$^7F_2$ is induced electric dipole allowed and depends strongly on the local symmetry around Eu^{3+} ion, this transition is extremely sensitive to ligand symmetry and bond covalence **[25]**, and tends to be much more intense in non-symmetric sites and high bond covalence. In contrast, the transition $^5D_0$-$^7F_1$ is magnetic dipole allowed and is independent on ligand symmetry and bond covalence. In the present work, the strongest emission intensity is for $^5D_0 \rightarrow {}^7F_2$ transition, corresponding to 616 nm intense red emission of the phosphor material. This observation indicates that local symmetry around Eu^{3+} ions in the $PNZFEu_{0.5}$ and $PNZFEu_{0.5}$ matrix is low, and thus the majority of Eu^{3+} ions are located in an asymmetric environment. The transitions from $^5D_0$ to $^7F_{0,3,5}$ are very weak because violate the selection rules, and hence are forbidden both in magnetic and induced electric dipoles schemes. It should be noted that the emission intensities of glasses are pronounced at room temperature, the annealed glass at 380 °C at 1 hour exhibit a large intensity compared to those at low temperature which may be due to the nanocrystallite phase formed in the annealed glass. The superposition of several emission spectra of samples excited at room and low temperature (Fig.5) and also at different wavelengths (Fig. 6) indicates that for the $^5D_0$-$^7F_0$ transition we observe only one peak, which explains the one dimensional site, while the magnetic dipole $^5D_0$-$^7F_1$ transition splits into three components, indicating that the crystallographic site of the Eu^{3+} ions in the present glasses is as low as orthorhombic, monoclinic or triclinic in a crystalline lattice **[26, 27]**. A very small shift is observed in stark level of these bands according to the change of wavelength. The energy level diagram for the emission mechanism of Eu^{3+} in the studied glasses is shown in Fig. 7.

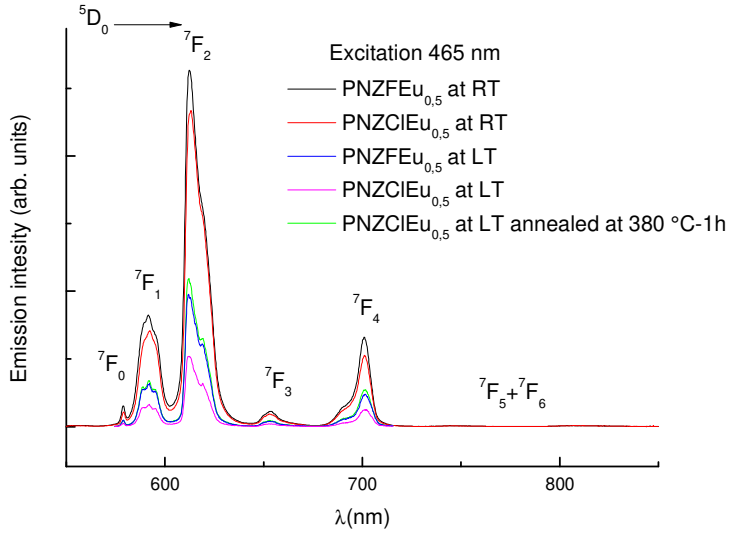

Figure 5 Luminescence spectra of PNZFEu$_{0.5}$, PNZClEu$_{0.5}$ glasses and PNZClEu$_{0.5}$ annealed glass at 380 °C for 1 hour at low and room temperature.

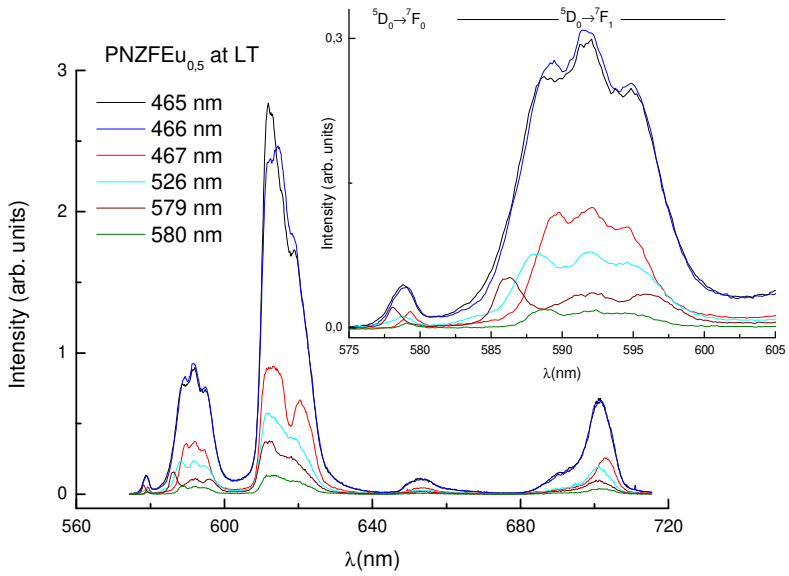

Figure 6 Emission spectra of PNZFEu$_{0.5}$ at low temperature excited at different wavelengths, The inset is a zoom in the 575-605 nm spectral range, showing wavelength dependence of the $^7F_{0,1}$ bands degeneracies.

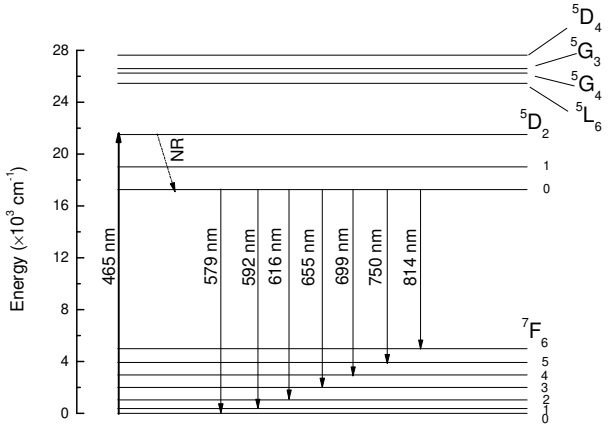

Figure 7 Emission mechanism of Eu^{3+}-doped $PNZFEu_{0.5}$ or $PNZClEu_{0.5}$ glasses.

J-O intensity parameters Ω_t (t = 2, 4, 6) are important indicators to predict some radiative properties such as oscillator strengths, luminescence branching ratios, energy-transfer probabilities, and excited-state radiative lifetime **[28]**, which are usually derived from absorption spectrum. Nevertheless, they were calculated from the emission spectrum due to the special energy level structure of Eu^{3+} in present work. The J-O analysis described in detail elsewhere **[29-32]**, and the results are gathered in Table 3. The intensity parameter Ω_2 has been identified to be associated with the asymmetry and the covalence between RE ions and ligand anions, and $\Omega_{4,6}$ parameters are related to the bulk property and rigidity of the samples, respectively. In both $PNZFEu_{0.5}$ and $PNZClEu_{0.5}$ glasses, the trend is as follows: $\Omega_2 > \Omega_4 > \Omega_6$. The larger value Ω_2 for glasses systems indicates stronger covalency of Eu–O bonds. The integrated fluorescence intensity ratio of $^5D_0 \rightarrow {}^7F_2/{}^5D_0 \rightarrow {}^7F_1$, the asymmetry ratio R, can be viewed as the spectroscopic key parameter to estimate the site asymmetry and the chemical bond covalency of Eu^{3+} ions **[33]**. The value of this asymmetry ratio is 3.5-4 in glasses, which is high and reveals a high local asymmetry and the formation of the strong Eu-O bond in the glasses, confirmed the line of reasoning above. Fig. 8 shows the glasses emission spectra, calibrated in cross section unit by the Fuchtbauer-Ladenburg (FL) method, at low and room temperature after excitation at 465 nm.

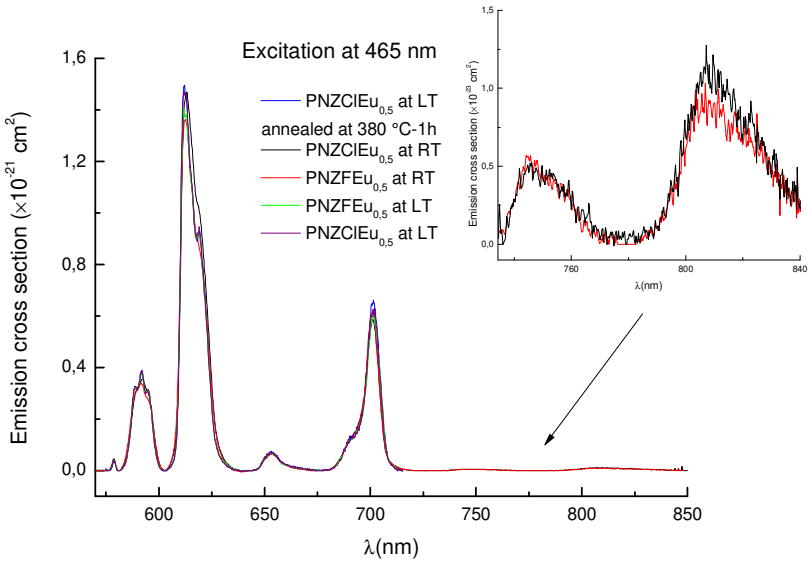

Figure 8 Stimulated emission cross-sections of $PNZFEu_{0.5}$ and $PNZClEu_{0.5}$ glasses calibrated by the Fuchtbauer-Ladenburg method, at room and low temperature. The inset is a zoom of the $^7F_{5,6}$ transitions cross sections.

Table 3 Results of the Judd-Ofelt analysis carried out in the $PNZFEu_{0.5}$, $PNZClEu_{0.5}$ and annealed $PNZClEu_{0.5}$ glasses: JO parameters ($\Omega_{2,4,6}$), electric and magnetic dipole oscillator strength (f), radiative transition rates (A_R), branching ratios (β_R), asymmetry ratio (R), radiative lifetimes (τ_R) and quantum efficiency (η).

Samples	Transitions	$\bar{\nu}(cm^{-1})$	$\Omega_2(\times10^{20}$ $cm^2)$	$\Omega_4(\times10^{20}$ $cm^2)$	$\Omega_6(\times10^{20}cm^2)$	$f\times10^{-6}$	A_R (s^{-1})	$\beta_R(\%)$	R	τ_R (ms)	η (%)
	$^5D_0\rightarrow{}^7F_0$	17280				0.0030	1.40	0.45			
	$\rightarrow{}^7F_1$	16900				0.12	54.08	17.66			
	$\rightarrow{}^7F_2$	16230				0.47	196.85	64.29			
$PNZFEu_{0.5}$**-RT**	$\rightarrow{}^7F_3$	15271	5.96	2.80	1.41	0.017	6.44	2.11	3.64	3.27	83.80
at 465 nm	$\rightarrow{}^7F_4$	14308				0.14	45.55	14.88			
	$\rightarrow{}^7F_5$	13336				0.0022	0.61	0.20			
	$\rightarrow{}^7F_6$	12280				0.0052	1.26	0.41			
	$^5D_0\rightarrow{}^7F_0$	17282				0.003	1.41	0.47			
	$\rightarrow{}^7F_1$	16899				0.12	54.07	18.05			
	$\rightarrow{}^7F_2$	16230				0.45	191.74	64.01			
	$\rightarrow{}^7F_3$	15258	5.80	2.78	--	0.02	7.10	2.37	3.54	3.34	77.84
$PNZFEu_{0.5}$**-LT**	$\rightarrow{}^7F_4$	14302				0.14	45.23	15.01			
at 465 nm	$\rightarrow{}^7F_5$	--				--	--	--			
	$\rightarrow{}^7F_6$	--				--	--	--			
	$^5D_0\rightarrow{}^7F_0$	17276				0.002	1.06	0.33			
	$\rightarrow{}^7F_1$	16894				0.12	54.03	16.75			
	$\rightarrow{}^7F_2$	16222				0.51	214.13	66.39			
$PNZClEu_{0.5}$ **-RT**	$\rightarrow{}^7F_3$	15266	6.49	2.74	1.65	0.018	6.57	2.04	3.96	3.10	80.32
at 465 nm	$\rightarrow{}^7F_4$	14309				0.14	44.63	13.84			
	$\rightarrow{}^7F_5$	13307				0.0022	0.64	0.20			
	$\rightarrow{}^7F_6$	12283				0.006	1.48	0.46			
	$^5D_0\rightarrow{}^7F_0$	17286				0.003	1.42	0.47			
	$\rightarrow{}^7F_1$	16899				0.12	54.08	17.79			
	$\rightarrow{}^7F_2$	16233				0.46	195.46	64.28			
$PNZClEu_{0.5}$ **-LT**	$\rightarrow{}^7F_3$	15259	5.92	2.41	--	0.02	7.40	2.43	3.61	3.29	77.20
at 465 nm	$\rightarrow{}^7F_4$	14302				0.14	45.71	15.03			
	$\rightarrow{}^7F_5$	--				--	--	--			
	$\rightarrow{}^7F_6$	--				--	--	--			
	$^5D_0\rightarrow{}^7F_0$	17284				0.003	1.30	0.42			
	$\rightarrow{}^7F_1$	16899				0.12	54.07	17.53			
	$\rightarrow{}^7F_2$	16231				0.47	197.23	63.95			
Annealed	$\rightarrow{}^7F_3$	15255	5.97	2.97	--	0.02	7.57	2.46	3.64	3.24	--
$PNZClEu_{0.5}$ **-LT-**	$\rightarrow{}^7F_4$	14303				0.15	48.21	15.63			
at 465 nm	$\rightarrow{}^7F_5$	--				--	--	--			
	$\rightarrow{}^7F_6$	--				--	--	--			

6. Crystal field analysis

Using phenomenological free-ion Hamiltonian (HFI) model **[34]**, energy level analysis has been carried out. The second and fourth rank crystal-field (CF) parameters have been evaluated by assuming a C_{2v} orthorhombic symmetry for the local environment of Eu^{3+} ions to estimate the CF strength parameter experienced by Eu^{3+} ions **[35-40]**. This approximation is made since a subgroup of almost all the higher order point groups which allow optical activity from the $^5D_0$ level to ^7F_J Stark levels and is the highest order noncentrosymmetric point group that removes complete degeneracy of the ^7F_J levels. Only 10 components $^5D_0$ and $^7F_{0,1,2}$ multiplets of 3003| *SLMJ}* Stark sublevels of the $4f^6$ configuration which constitute the truncation of the wave function is taken account. The restricted set of wave functions has in most cases been found sufficient to describe in an adequate way the effect of the neighboring atoms on the electronic structure of the Eu^{3+} ion.

The energies of the Stark levels of the $^7F_1$ and $^7F_2$ multiplets were obtained from the experimental emission spectrum recorded at 77 K by Gaussian deconvolution of the respective bands presented in fig 9 .The energy difference between the extreme Stark levels for the $^7F_1$ and $^7F_2$ levels are comparable in both glasses. From the Stark level positions of the $^7F_1$ and $^7F_2$ multiplets, CF analysis has been carried out, to know the variation of CF strength acting on the Eu^{3+} ions in glasses. The CF analysis was carried out using Wybourne's formalism **[41].** The relevant CF parameters *Bkq* were obtained by giving the best fitting between the experimental and calculated splittings of the $^7F_1$ and $^7F_2$ multiplets of Eu^{3+} ions (see table 4). To estimate the quality of the fit, the root-mean-square (r.m.s.) deviation referred as standard deviation (σ) has been determined and found to be ±3.35, 2.40 cm^{-1} for $PNZFEu_{0.5}$ and $PNZClEu_{0.5,}$ respectively which reveals that good fit between observed and calculated energies **[42].** The CF parameters B_q^k and their ratios B_2^2/B_0^2 and B_4^4/B_0^4 for the present glasses, are presented in Table 5 along with similar parameters for the PKBAFEu10, PKBAEu10 and PKSAEu10 glasses for comparison**[2-3, 40].** The ratios B_2^2/B_0^2 and B_4^4/B_0^4 change dramatically and care should be taken when comparing with other results. We can notice that the CF parameters are comparable with those reported Eu^{3+} phosphates glass systems **[2-3,40]**.In order to compare the crystal field strength exerted around the Eu^{3+} 4f electrons in the $PNZFEu_{0.5}$ and $PNZClEu_{0.5}$ glasses, with similar phosphate materials **[2-3,40]**, we calculated the scalar CF strength parameter S **[43]** , as follows:

$$s = \left\{ \frac{1}{3} \sum_k \frac{1}{2k+1} \left(\left| B_0^k \right|^2 + 2 \sum_{q>0} \left| \mathrm{Re}\, B_q^k \right|^2 + \left| \mathrm{Im}\, B_q^k \right|^2 \right) \right\}^{1/2} \qquad (3)$$

We found that S=296 cm^{-1} in the $PNZFEu_{0.5}$ glass and S=287 cm^{-1} in the $PNZClEu_{0.5}$ glass. These values are slightly less than phosphate glasses reported in **[2-3, 40]** works. The higher crystal field strength is due to the larger charge density and/or smaller Eu-O distance **[2, 44]** while low S value can be attributed to the reduction in charge density and/or increase in the Eu–O distance **[45]**.

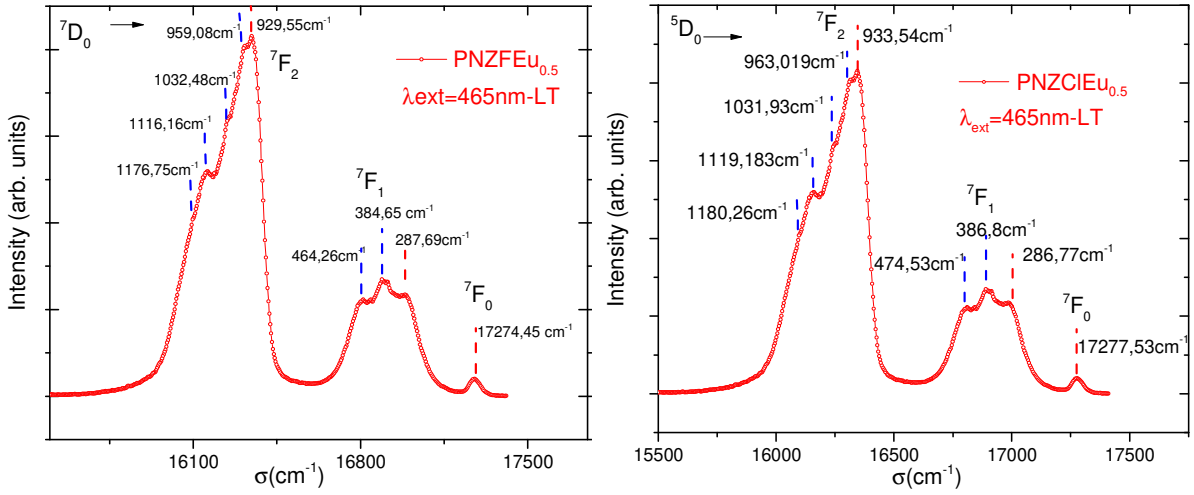

Figure 9 $^5D_0 \rightarrow {}^7F_{0,1,2}$ Stark level splittings of $PNZFEu_{0.5}$ and $PNZClEu_{0.5}$ glasses.

Table 4 Comparison of experimental and calculated crystal-field levels for Eu^{3+} ions in PNZF and PNZCl glasses. All numbers are in cm^{-1}.

$^{2S+1}$Lj Crystal field levels	PNZFEu$_{0.5}$		PNZClEu$_{0.5}$	
	E_{exp}	E_{cal}	E_{exp}	E_{cal}
$^7F_0$	0.0	0.1	0.0	0.8
$^7F_1$	274.3	279.1	284.4	287.1
	380.7	379.8	391.7	392.3
	499.5	495.6	493.8	490.8
$^7F_2$	904.5	900.0	903.4	899.3
	940	944.4	935.5	938.3
	984.1	980.6	977.3	974.4
	1047.2	1046.6	1035.9	1036.5
	1161.0	1165.4	1149.7	1152.9
$^5D_0$	17280	17280.0	17277.0	17277.0
σ (N)[(a)]		3.35(10)	2.40(10)	

(a): "**σ"** indicates root mean-square deviation between experimental and calculated values; **"N"** indicates number of levels used in the fitting.

Table 5 Calculated sets of crystal-field B^k_q parameters and CF strength parameter (S) for the C_{2v}-point group symmetry in the samples PNZFEu$_{0.5}$ and PNZClEu$_{0.5}$, compared with those of some known host. All numbers are in cm^{-1}.

B^k_q	PNZFEu$_{0.5}$	PNZClEu$_{0.5}$	PKBAEu10 [2]	PKBAFEu10 [3]	PKSAEu10[41]
B_0^2	-550.825	-537.992	-314	-306	-479
B_2^2	-230.285	-196.010	-168	-215	-119
B_0^4	576.100	546.194	865	990	1321
B_2^4	12.199	37.344	358	292	275
B_4^4	-807.250	-793.882	-1073	-1100	-731
B_2^2/B_0^2	0.418	0.36	0.54	0.70	0.24
B_4^4/B_0^4	-1.40	-1.45	-1.24	-1.11	-0.55
S	296	287	364	380	396

7. Fluorescence decays

The luminescence decays of the $^5D_0 \rightarrow {}^7F_2$ transition at low and room temperature in PNZFEu$_{0.5}$ and PNZClEu$_{0.5}$ excited state to its lower lying energy levels have been recorded monitoring the excitation and emission wavelengths at 465 nm and 612 nm, respectively. Due to the large energy gap between the $^5D_0$ and $^7F_6$ (~12000 cm^{-1}) as shown in **Figure 7**, the lifetime of $^5D_0$, usually on the order of milliseconds, does not vary significantly below room temperature (300 K). The fluorescence decay from $^5D_0$ of Eu^{3+} ions at normal sites is generally single exponential with an initial buildup time varying from μs to ms in different hosts due to nonradiative relaxation from $^5D_1$ and upper states[**46**]. As seen from **Figure. 10**, it is clear that the decay profiles are almost single exponential and are very similar for both systems. Mostly, the fluorescence intensity emitted by rare earth ions doped glasses varies with the composition of the glass host **[47]** and the concentration of the rare earth ions. Indeed, some authors reported that if Eu^{3+} ion concentration increases beyond 1.0 *mol%* **[48-50],** or 2 *mol %* **[51]** then the decrease in luminescence intensity (concentration quenching) is observed.

The quantum efficiency η for $^5D_0$ level can be calculated using the fluorescent lifetime τ_{exp} and the radiative transition rate τ_{rad} through the relation

$$\eta = \frac{\tau_{mes}}{\tau_{rad}} \qquad (4)$$

For both glasses the quantum efficiencies are less than unity, which is clearly due to manifestation of the non-radiative process. On the other hand, the glasses present high quantum efficiencies (**nearly 80 %**) which are a consequence of the absence of major non-radiative channels such as multi phonon relaxation, cross-relaxation and the expected lower phonon energies. This value is higher than (~48%) reported in $Li_2B_4O_7$:0.5Eu and

CaB_4O_7:0.5Eu glasses **[52],** and very close to commercial Y_2O_3 phosphor (~95%) **[53]**.The energy storage ($G=\sigma_{em}\times\tau_{exp}$) is critical parameter used to predict probable lasing emission transition of Eu^{+3} ions. The stimulated cross section describes maximum spatial optical amplification which can be an important parameter in development of high gain and low threshold laser applications, while the optical gain design highly efficient and stable laser active materials. The optical gain parameter for the red emission ($^5D_0\rightarrow{}^7F_2$) is equal to 3.66×10^{-24} cm^2.s which is practically identical with RLTB **[54]**. It worth to mention that red emissions exhibit good laser parameters that make the glasses host matrix as a good laser candidate for these visible emission.

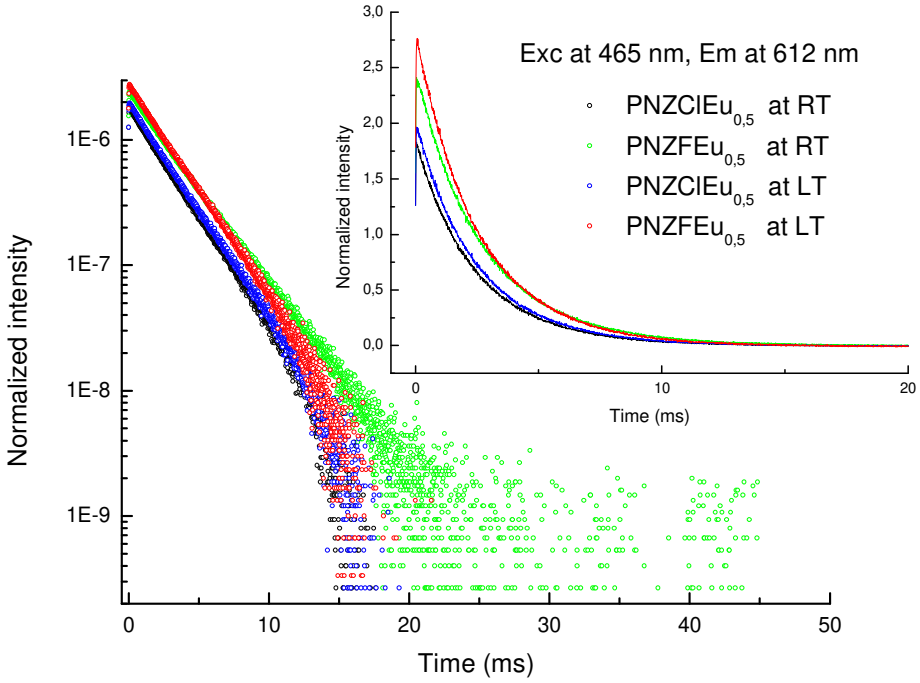

Figure 10 Fluorescence decays measured in the $PNZFEu_{0.5}$ and $PNZClEu_{0.5}$ glasses at low and room temperature.

8. Conclusions

Oxyfluoro-phosphate and oxychloro-phosphate glasses containing Eu^{3+}-ions have successfully developed and shown good optical quality, moisture resistant and more stable.

The electronic structure of Eu^{3+} ions in phosphate glasses has been analyzed from absorption and emission spectra by means of a model Hamiltonian. Stark splittings of $^5D_0$-$^7F_{1,2}$ transitions have been used to estimate the *Bkq* parameters. The number of Stark levels suggests that the Eu^{3+} ion site in the title glasses can be described by a local C_{2v} symmetry. The crystal- field strength has been calculated and found that it varies with host composition.

The JO parameters have been derived by analyzing emission spectrum for glasses measured at low and room temperature and are found to be relatively more reliable, which are used to predict radiative properties for $^5D_0$ level of Eu^{3+} ions. A relatively higher value of the intensity parameter Ω_2 indicates higher covalence and/or higher asymmetry around Eu^{3+} ions in the present host. The decay profiles of the $^5D_0$ level of Eu^{3+} ions in the studied glasses are found to be single exponential indicating the almost absence of energy transfer between Eu^{3+} ions in the present glass host.

Relatively large stimulated emission cross-section, high branching ratios and quantum efficiencies confirm that the present glasses with Eu^{3+} ions emits intense red luminescence at 616 nm by suggesting $PNZFEu_{0.5}$ and $PNZClEu_{0.5}$ glasses are the good materials for optical devices.

Acknowledgments

Samah Amrouch is the owner of a PNE program fellowship of the Algerian Ministry of Higher Education and Research. She also thanks the French CMDO+ network of the MITI-CNRS for an ITC mobility fellowship. We thank Thierry Encinas, Rachel Martin and Florence Robaut for technical assistance in XRD, SEM-EDX and EPMA-EDS analysis.

References

[1] C. Gorller-Walrand, K. Binnemans, in: K.A. Gschneidner Jr.,L. Eyring (Eds.), Handbook on the Physics and Chemistry of Rare Earths, vol. 25, North-Holland, Amsterdam, 1998 (Chapter 167).
[2] S. Surendra Babu, P. Babu, C.K. Jayasankar, W. Sievers, Th. Troster, G. Wortmann, J. Lumin. 126 (2007) 109.
[3] R. Balakrishnaiah, R. Vijaya, P. Babu, C.K. Jayasankar, M.L.P. Reddy, J. Non- Cryst. Solids 353 (2007) 1397.
[4] A.Y. Hamad, J.P. Wicksted, Appl. Opt. 40 (2001) 1822–1826.
[5] Ch.S. Rao, K.Upendra U. Kumar, C.K. Jayasankar, Solid State Sci. 13 (2011) 1309–1314.
[6] J. Anjaiah, C. Laxmikanth, N. Veeraiah, Physica B 454 (2014) 148–156.
[7] V. Hegde, A. Wagh, H. Hegde, C.S.D. Vishwanath, S.D. Kamath, Appl. Phys. A 302 (2017) 1–13.
[8] M. De, S. Sharma, S. Jana, Physica B 556 (2019) 131–135.
[9] G.H. Silva, V. Anjos, M.J.V. Bell, A.P. Carmo, A.S. Pinheiro, N.O. Dantas, J. Lumin. 154 (2014) 294–297.
[10] P.Y.Shih,S.W.Yung ,C.Y.Chen ,H.S.Liu,T.S.Chin, Mater .Chem.Phys .50 (1997) 63-69.
[11] R.K.Brow, J.Non-cryst.Solids 263 (2000) 1-28.
[12] P.A.Tick, Phys .chem.Glasses 25(1984) 149.
[13] S.S.Das, B.P.Baranwal,C.P.Gupta, Punita Singh, J.Power Sources 114 (2003) 346-351.
[14] P.Y.Shih,S.W.Yung ,C.Y.Chen ,H.S.Liu,T.S.Chin, Mater .Chem.Phys .50 (1997) 63-69.
[15] J. Anjaiah, C. Laxmikanth, N. Veeraiah, Physica B 454 (2014) 148–156.
[16] V. Hegde, A. Wagh, H. Hegde, C.S.D. Vishwanath, S.D. Kamath, Appl. Phys. A 302 (2017) 1–13.
[17] V. Chandrappa, Ch. Basavapoornima , C.R. Kesavulu, A. Mohan Babu , Shobha Rani Depuru , C.K. Jayasankar J.Non-Cryst.Solids 583 (2022) 121466.
[18] D.R. Uhlmann, J.Non-Cryst.Solids 25 (1977) 42.
[19] S.Chaguetmi, A.Boutarfaia, M.Poulain; J. optoelectronics advanced materials, 15 (7-8), (2013) , 605-609.
[20] S.H. Bindu, D.S Raju, V.V Krishna, T.R Rao, K. Veerabrahmam, Ch.L. Raju, Opt. Mater. 62 (2016) 655–665.
[21] A.Maity, S.Jana,S.Ghosh,S.Sharma, J.Non-Cryst.Solids 550 (2020) 120322.
[22] S. Selvi, K. Marimuthu, G. Muralidharan, J. Mol. Struct. 1144 (2017) 290–299.
[23] E.A. Davis, N.F. Mott, Philos. Mag. 22 (1970) 0903–0922.
[24] G. Seeta Rama Raju, H.C. Jung, J.Y. Park, B.K. Moon, R. Balakrishnaiah, J.H. Jeong, J.H. Kim, Sens. Actuators B Chem. 146 (2010) 395–402.
[25] G. Lakshminarayana, E. M. Weis, A. C. Lira, U. Caldiño, D. J. Williams, and M. P. Hehlen, J. Lumin. 139, (2013) 132–142.
[26] J. Fernandez, R. Balda, J.L. Adam, J. Phys.: Condens. Matter 10 (1998) 4985.
[27] C. Görller-Walrand, K. Binnemans, in: K.A. Gschneidner Jr., L. Eyring (Eds.), Handbook on the Physics and Chemistry of Rare Earths, vol. 23, North-Holland, Amsterdam, 1996 (Chapter 155).
[28] M. P. Hehlen, M. G. Brik, and K. W. Krämer, J. Lumin. 136, (2013) 221–239.
[29] R. Belhoucif, M. Velazquez, Y. Petit, O. Plantevin, M.A. Couto dos Santos, F. Adamietz, V. Rodriguez, M. Couzi, O. P_erez, O. Viraphong, P. Veber, D. Denux, R. Decourt, D. Ouadjaout, Opt. Mater. Express. 4 (10) (2014) 2042-2065.
[30] P.Veber, M.Velazquez, P.A.Douissard, T.Martin, O. Plantevin, and R.Belhoucif, Opt. Mater. Express. 6 (1) (2016) 207-219.
[31] R.Belhoucif, M.Velázquez, O.Plantevin, P.Aschehoug, P.Goldner, G.Christian, Opt. Mater. 73 (2017), 658- 665.
[32] R.Belhoucif, M.Velazquez, O.Plantevin, P.Aschehoug, P.Goldner, G.Christian, AIP Conf. Proc. 1994, (ICRA-2017) 030002-1–030002-6.

[33] K. Upendra Kumar, S. Surendra Babu, Ch. Srinivasa Rao and C.K. Jayasankar, Opt. Commun., 2011, 284, 2909–2914.
[34] W.T. Carnall, G.L. Goodman, K. Rajnak, R.S. Rana, J. Chem. Phys. 90 (1989) 3443–3457.
[35] C. Brecher, J. Chem. Phys. 61 (1974) 2297.
[36] C. Brecher, L.A. Riseberg, Phys. Rev. B 21 (1980) 2607.
[37] C. Brecher, L.A. Riseberg, Phys. Rev. B 13 (1976) 81.
[38] C. K. Jayasankar, K. Ramanjaneya Setty, P. Babu,Phys Rev B 69 (21), 214108 (2004)
[39] V. Venkatramu , D. Navarro-Urrios , P. Babu,C.K. Jayasankar, V. Lavin, J.Non-Cryst.Solids 351 (10-11), 929-935 (2005).
[40] K.Linganna, C.K. Jayasankar, Spectrochimica Acta Part A: Molecular and Biomolecular Spectroscopy 97 (2012) 788–797.
[41] B.G. Wybourne, Wiley-Interscience, New York, 1965.
[42] C.A. Morrison, R.P. Leavitt, in: K.A. Gschneidner, L. Eyring (Eds.), Handbook on Physics and Chemistry of Rare Earths, vol. 5, North-Holland Publishing Co., Amsterdam, 1982, pp. 461–692.
[43] N.C. Chang, J.B. Gruber, R.P. Leavitt, C.A. Morrison, J. Chem. Phys. 76 (1982) 3877.
[44] Ch. Srinivasa Rao, K. Upendra Kumar, C.K. Jayasankar, Solid State Sciences 13 (2011) 1309-1314.
[45] V. Lavin, P. Babu, C. K. Jayasankar, I. R. Martin, and V. D. Rodriguez, J. Chem. Phys. 115, 10935 (2001).
[46] X.Y. Chen, G.K. Liu, J. Solid State Chemistry 178 (2005) 419–428.
[47] W.A. Pisarski, J. Pisarska, G. Dominiak-Dzik, M. Maczka, W. Ryba-Romanowski, J. Phys. Chem. Solids 67 (2006) 2452–2457.
[48] N. Sooraj Hussain, Y. Prabhakara Reddy, S. Buddhudu, Mater. Res. Bull. 36 (2001) 1813–1821.
[49] A.Kumar, D.K. Rai, S.B. Rai, Spectrochim. Acta A 58 (2002) 2115–2125.
[50] K.K. Mahato, S.B. Rai, A. Rai, Spectrochim. Acta A 60 (2004) 979–985.
[51] B.C. Jamalaiah, J. Suresh Kumar, A. Mohan Babu, L. Rama Moorthy, J. Alloys Compd. 478 (2009) 63–67.
[52] I.I. Kindrat , B.V. Padlyak , Opt. Mater. (2018) 77, 93-103
[53] W.D.A.M. de Boer, C. McGonigle, T. Gregorkiewicz, Y. Fujiwara, S. Tanabe, P. Stallinga , Sci. Rep. (2014) 4, 5235.
[54] S.A. Saleem, B.C. Jamalaiah, A. Mohan Babu, K. Pavani, L. Rama Moorthy, J. Of Rare Earths, Vol. 28, No. 2, (2010), p. 189.